receiver is decision-aided, 'runaways' are prevented by sending ten known symbols after every 1000 symbols. The BEP results are shown in Fig. 3 for BPSK and QPSK. With a constant carrier phase, the simulated performance is indistinguishable from that of the coherent receiver, which is $\frac{1}{2}$ erfc $[E_b/N_0]^{1/2}$ for both BPSK and QPSK. (E_b is the energy per bit. Thus, $E_b = E_s$ for BPSK and $E_b = E_s/2$ for QPSK.) For a time-varying phase, the performance loss compared to coherent performance is higher for QPSK than for BPSK. Performance loss due to errors in the decisions fed back to the reference $\tilde{v}(k)$ in eqn. 5 and the adaptation algorithm (eqn. 8) is only noticeable for low SNR. For comparable values of σ in eqn. 9 and $\Delta\theta$ in eqn. 10, the linearly-increasing phase model leads to a greater degradation of performance compared to the random-walk model. The choice of β only affects the BEP performance at low SNR, but not at high SNR. Extensive simulations indicate that $\beta = 1$ is nearly optimum at high SNR for a wide range of values of σ^2 and $\Delta\theta$. No hang-ups during the initial acquisition period or cycle slips during steady state operation were observed in the simulations.

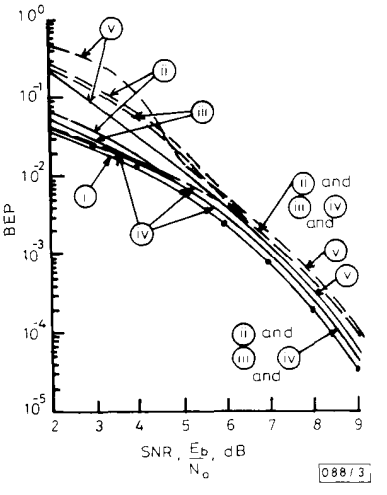

Fig. 3 *Simulated bit error probability of 2- and 4-PSK with coherent reference(s)*

(i) Coherent (theoretical)—$\frac{1}{2}$ erfc $\left[\frac{E_b}{N_0}\right]^{1/2}$

● Constant unknown phase

Gaussian random-walk phase, $\sigma^2 = 0{\cdot}005$ rad^2 for 2PSK, $\sigma^2 = 0{\cdot}001$ rad^2 for 4PSK

(ii) $\beta = 1$, (iii) $\beta = 0{\cdot}99$ } Detected *symbols* fed back

(iv) $\beta = 1$ ideal decision feedback

(v) Linearly increasing phase, detected symbols fed back, $\Delta\theta = 0{\cdot}05$ rad for 2PSK, $\Delta\theta = 0{\cdot}01$ rad for 4PSK

——— 2-PSK

- - - - 4-PSK

Besides its simplicity and excellent performance, our receiver is robust with respect to the carrier phase process. By comparison, an extended Kalman filter estimator of carrier phase, as proposed in Reference 2, only applies to a Gauss–Markov phase model such as eqn. 9, and the setting of the Kalman gain requires knowledge of the model parameters such as σ^2. The latter estimator cannot be applied to the linearly-increasing phase model (eqn. 10).

Acknowledgment: Pranesh Sinha is the recipient of a Motorola Partnership in Research and Development Augmentation Award.

18th August 1992

P. Y. Kam, P. Sinha and A. M. C. Kan (*Department of Electrical Engineering, National University of Singapore, 10 Kent Ridge Crescent, Singapore 0511, Republic of Singapore*)

References

1 KAM, P. Y.: 'Maximum likelihood carrier phase recovery for linear suppressed-carrier digital data modulations', *IEEE Trans.*, 1986, **COM-34**, pp. 522–527

2 AGHAMOHAMMADI, A., MEYR, H., and ASCHEID, G.: 'Adaptive synchronization and channel parameter estimation using the extended Kalman filter', *IEEE Trans.*, 1989, **COM-37**, pp. 1212–1219

TUNABLE MEMBERSHIP FUNCTION CIRCUIT FOR FUZZY CONTROL SYSTEMS USING CMOS TECHNOLOGY

J.-J. Chen, C.-C. Chen and H.-W. Tsao

Indexing terms: Control theory, Fuzzy logic

The membership function circuit (MFC) is used in the input parts of analogue fuzzy hardware systems. The fuzzy hardware can execute singleton fuzzy control algorithms. In the letter a voltage-input current-output membership function circuit is proposed. The characteristic of this building block is tunable and is useful for current-mode analogue fuzzy hardware. The proposed circuit was designed by using 3·5 μm CMOS design rules, and its operations have been confirmed using PSPICE simulations.

Introduction: Recently, fuzzy theory has been applied effectively to automatic control and expert systems. A feature of fuzzy theory is that uncertain linguistic information can be handled quantitatively by using membership functions. In addition to theoretical studies, the hardware implementations of fuzzy information systems have been studied to realise high-speed operations and reduce system size. The current-mode circuits can satisfy this requirement, and they are not sensitive to changes of supply voltages. However, they have a weakness that the fan-out number is restricted to only one. This weakness gives rise to considerable problems in input parts of fuzzy hardware systems since the inputs must be distributed to many operational blocks. So in this letter a voltage-input current-mode membership function circuit is proposed and the simulation of this circuit is given.

Circuit description: A membership function is one of the most important circuits for a fuzzy control system. In this letter the MFC is designed to have voltage input and current output. The voltage input can be easily distributed to many rule blocks which have the MFC in the input parts. To introduce the proposed circuit, first we discuss the floating voltage-controlled resistors shown in Fig. 1. The equivalent resistance R_{12} between nodes V_1 and V_2 can be derived as [1]

$$R_{12} = \left[2\mu_p C_{ox}\left(\frac{W}{L}\right)_p (V_C - |V_{TP}|)\right]^{-1} \quad (1)$$

where V_{TP} is the threshold voltage of the PMOS transistor and $(W/L)_p$ is its aspect ratio. These integrable resistors are used to construct source resistors of a CMOS operational transconductance amplifier (OTA), and these resistors can

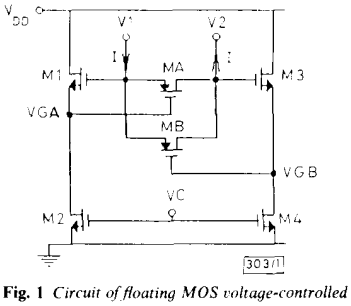

Fig. 1 *Circuit of floating MOS voltage-controlled resistor*

change the transconductance G_m of an OTA with variable R_{12}. The saturation current of this OTA is a constant when the bias current is not changed. This characteristic is useful for an MFC. The proposed MFC is built with these OTAs and is illustrated in Fig. 2. The transfer curve of this MFC is related

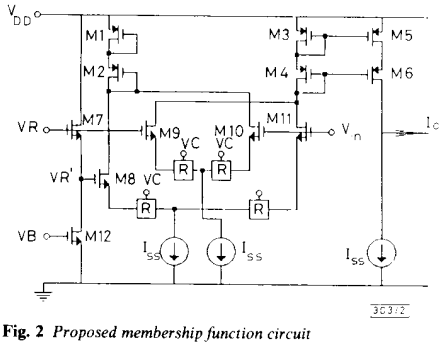

Fig. 2 *Proposed membership function circuit*

to the parameters shown in Fig. 3. The reference voltage V'_R depends on V_R and can be derived as [2]

$$V_R = V_R - V_B \tag{2}$$

When the input voltage V_{in} approaches V'_R and V_R, the output current I_0 can be obtained as follows:

$$I_0 \approx \frac{I_{ss}}{2} + G_m[V_{in} - V'_R] \qquad \text{when } V_{in} \text{ approaches } V'_R \tag{3}$$

$$I_0 \approx \frac{I_{ss}}{2} - G_m[V_{in} - V_R] \qquad \text{when } V_{in} \text{ approaches } V_R \tag{4}$$

where

$$G_m = \frac{1}{2\left\{\left[\frac{1}{2\mu_n C_{ox} I_{ss}}\left(\frac{L}{W}\right)_n\right]^{1/2} + R_{12}\right\}}$$

We can change the slope G_m of the transfer curve through R_{12} by varying V_C. The voltages V_B and V_R determine the width and horizontal position of the transfer curve, respectively. The height of the curve is controlled by the bias current I_{ss}. For suitable V_B and V_C, the maximum output current will take place and approach I_{ss} when input voltage V_{in} is equal to $0{\cdot}5(V_R - V'_R)$. If V_{in} is greater than $V_R + 0{\cdot}5V_B$ or less than $V'_R - 0{\cdot}5V_B$, the current I_0 will approach zero.

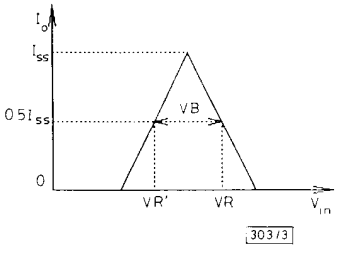

Fig. 3 *Characteristic of general membership function*

This MFC will be simulated by using PSPICE in the following Section. In Fig. 2 the proposed circuit was designed by using 3·5 μm CMOS design rules. The aspect ratios of M1–M6 and M7–M12 are, respectively, 30 μm/5 μm and 10 μm/5 μm. All the aspect ratios of MOS transistors in the floating voltage-controlled resistors are 5 μm/5 μm. The power supply voltage V_{DD} is 10 V.

Simulation results: In the preceding Section we have presented the circuit configuration of the membership function circuit. The simulation results of the membership function with variable widths and slopes are shown in Fig. 4. The parameter of each curve is listed as the following:

curve (1): $V_B = 2{\cdot}3$ V, $V_R = 6{\cdot}15$ V, $V_C = 1{\cdot}3$ V and $I_{ss} = 10\,\mu$A
curve (2): $V_B = 1{\cdot}6$ V, $V_R = 5{\cdot}8$ V, $V_C = 1{\cdot}8$ V and $I_{ss} = 10\,\mu$A
curve (3): $V_B = 1{\cdot}2$ V, $V_R = 5{\cdot}6$ V, $V_C = 5$ V and $I_{ss} = 10\,\mu$A

All the maximum output currents of the three curves occur at $V_{in} = 5$ V as required. The simulation results of MFC with

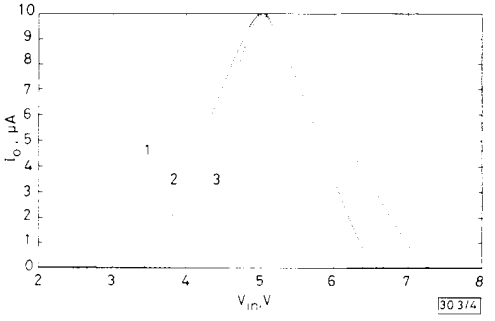

Fig. 4 *Membership function with variable widths*

variable horizontal positions are shown in Fig. 5. The reference voltages V_R are 5·1 V, 5·6 V and 6·1 V, respectively, for curves (1), (2) and (3). The other parameters are the same as curve (3) of Fig. 4. Furthermore, we can change the height of the membership function by varying the bias current I_{ss}, and the results are shown in Fig. 6. The bias currents are 10 μA, 7·5 μA and 5 μA, respectively, for curves (1), (2) and (3). The simulation results of this MFC have thus been obtained as expected.

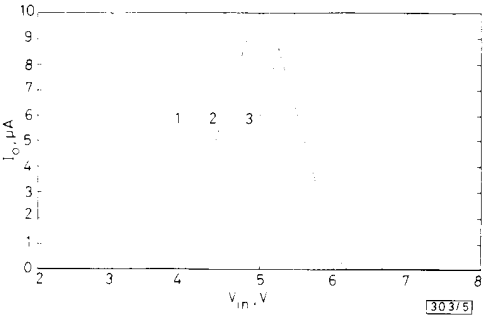

Fig. 5 *Membership function with variable horizontal positions*

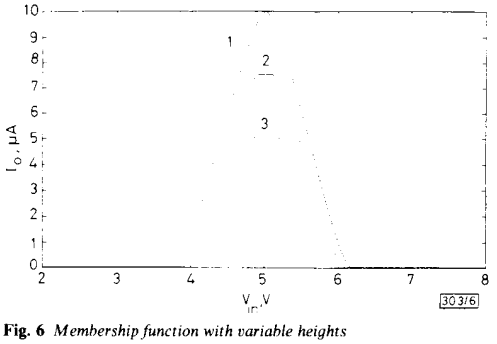

Fig. 6 *Membership function with variable heights*

Conclusion: A tunable membership function circuit for analogue fuzzy hardware systems using CMOS technology is proposed. The voltage inputs can be easily distributed to many rule blocks which have the MFC in the input parts. It is suitable to realise high-speed operations and small-size systems.

8th September 1992

J.-J. Chen, C.-C. Chen and H.-W. Tsao (*Department of Electrical Engineering, National Taiwan University, Taipei, Taiwan, 10764 ROC*)

References

1 BANU, M., and TSIVIDIS, Y.: 'Floating voltage-controlled resistors in CMOS technology', *Electron. Lett.*, 1982, **18**, (15), pp. 678–679
2 WANG, Z.: 'A CMOS four-quadrant analog multiplier with single-ended voltage output and improved temperature performance', *IEEE J. Solid-State Circuits*, 1991, **26**, (9) pp. 1293–1301
3 SEDRA, A. S., and SMITH, K. C.: 'Microelectronic circuits' (New York: HRW, 1987), 2nd edn.
4 TOGAI, M., and CHIU, S.: A fuzzy logic accelerator and a programming environment for real-time fuzzy control'. Proc. 2nd Inter. Fuzzy Systems Association Congress, July 1987, pp. 147–151
5 TOGAI, M., and WATANABE, H.: Expert system on a chip: an engine for real-time approximate reasoning', *IEEE Expert*, Fall, 1986, pp. 56–62

FIBRE-OPTIC PSK SUBCARRIER TRANSMISSION AT 35 GHz USING A RESONANTLY ENHANCED SEMICONDUCTOR LASER

S. Levy, R. Nagarajan, A. Mar, P. Humphrey and J. E. Bowers

Indexing terms: Semiconductor lasers, Fibre optics, Millimetre wave modulation

The authors investigate the characteristics of directly modulated semiconductor lasers using a 35 GHz subcarrier. They have achieved bit error rates of 10^{-10} for data transmission over short optical fibre links with a 35 GHz subcarrier.

Millimetre (mm) wave modulation of semiconductor lasers is of great interest for radar, communications, satellite links and electronic warfare systems. Applications include the processing and distribution of hundreds of antenna element signals in phased array radars, antenna remoting, delay lines and signal distribution. Optical fibre technology offers many advantages, such as high bandwidth, low loss, low weight, low dispersion, flexibility of the transmission medium and immunity to EMI and lightning. Optical fibres can serve as an excellent replacement for mm-wave waveguides [1–3]. However, application to mm-wave systems has not been possible because the largest direct modulation bandwidth reported to date in diode lasers is only 28 GHz [4].

Many mm-wave systems require only narrow bandwidth at centre frequencies much higher than the presently attainable direct modulation bandwidth of a laser diode. These systems will benefit from efficient narrow-band modulation techniques at frequencies above the intrinsic laser modulation bandwidth. References 5 and 6 discuss the possibility of modulating semiconductor lasers at mm-wave frequencies, even in the presence of electrical parasitics. In this paper we will present the results of a transmission system experiment using a mm-wave subcarrier at 35 GHz modulating a 1280 nm laser diode whose mm-wave response has been resonantly enhanced in an external cavity configuration. This laser diode had a maximum direct modulation bandwidth of only 15 GHz.

The experimental lightwave and mm-wave system is shown in Fig. 1. In the transmitter a 17·5 GHz synthesised signal (HP 8340B) is amplified and frequency doubled to generate the 35 GHz subcarrier. A waveguide balanced mixer is used to modulate the subcarrier with non-return-to-zero (NRZ) bipolar data output from an HP 70841B pattern generator. The result is a binary phased shift keyed (BPSK) signal centred at 35 GHz. The signal is amplified with a travelling wave tube (TWT) amplifier to 16 dBm and filtered to reduce the amplifier noise. A DC bias current is added to this signal and applied to intensity modulate the 1280 nm buried crescent laser [7]. The light from the antireflection coated rear facet is coupled to a gold mirror to form the external cavity and the front facet is coupled to single-mode silica fibre through an adjustable optical attenuator. The external cavity length is tuned to the third harmonic at 35 GHz.

At the receiver the light is detected with a PIN detector (HP 83440D). The −3 dB electrical bandwidth of the detector is 24 GHz and there is a 7 dB rolloff in the power response at 35 GHz. The DC responsivity of the photodetector is 0·5 A/W at 1300 nm. The output is band pass filtered and amplified, with a low noise mm-wave amplifier/mixer module, and down shifted to a 5 GHz intermediate frequency (IF) using a 30 GHz synthesised local oscillator (LO) source. A 15 GHz synthesiser (HP 8340B) source is cascaded with a power amplifier and frequency doubler to form the 30 GHz LO. The 10 MHz reference for this is provided by the transmitter. The resulting IF signal is amplified and down shifted to base-band, with a second LO at 5 GHz. The baseband signal is low-pass filtered and fed to the HP 70842B error detector to measure the bit error rate.

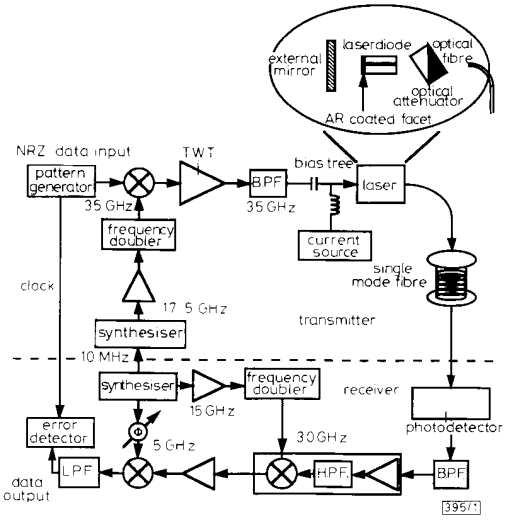

Fig. 1 *Block diagram of mm-wave subcarrier fibre optic transmitter/receiver system using a resonantly enhanced semiconductor laser*

Several requirements must be met for successful data transmission. The resonantly enhanced laser bandwidth at the resonance frequency will set an upper limit to the bit rate. The measurements and the analysis carried out in Reference 5 suggested a bandwidth of only a few tens of megahertz. In a recent analysis* a much larger bandwidth has been calculated. The second requirement is the laser AM noise. The intensity noise is also strongly peaked at the resonant frequency*. For a short optical link the laser AM noise will determine the received noise level and set the lower limit on the modulation power in order to achieve the minimum signal to noise ratio (SNR). The third requirement is the intermodulation distortion due to nonlinearities in the laser, detector and fibre generated by laser chirping and dispersion. The randomly modulated BPSK signal will generate distortion due to the third order intermodulation products in the system [8]. The laser is multimoded and lased at 1280 nm. The signal bandwidth combined with transmission in a 1312 nm zero dispersion fibre causes dispersion penalty, and sets the upper limit on the fibre length for a 10^{-9} bit error rate.

The system −3 dB bandwidth at the 35 GHz resonant peak was measured to be 0·7 GHz at 7·46 mW laser power output. For a 10 dBm 35 GHz CW input signal, we measured a 90 dB/Hz signal to laser intensity noise ratio. The two tone third order input intercept point at 35 GHz was measured to be 17 dBm. The system is currently limited by laser AM noise.

Typical transmission results are shown in Figs. 2 and 3. The spectrum of the detected optical signal is shown in Fig. 2 for a 35 GHz subcarrier and a 40 Mb/s BPSK signal. The eye diagram of the demodulated data after 200 m of fibre is shown as an inset. There is good eye opening. Fig. 3 shows the bit

* NAGARAJAN, R., LEVY, S., MAR, A., and BOWERS, J. E.: 'Resonantly enhanced semiconductor lasers' (in preparation)